Chemical Engineering Journal 500 (2024) 156634

Contents lists available at ScienceDirect

Chemical Engineering Journal

journal homepage: www.elsevier.com/locate/cej

Unlocking glycerol Potential: Novel pathway for hydrogen production and Value-Added chemicals

Alessandra Di Nardo [a,*], Gianluca Landi [b], Giuseppina Luciani [a], Maria Portarapillo [a], Giovanna Ruoppolo [b], Danilo Russo [a], Armando Zarrelli [c], Almerinda Di Benedetto [a]

[a] Department of Chemical, Materials and Production Engineering, University of Naples Federico II, P. le Tecchio 80, Naples 80125, Italy
[b] Istituto di Scienze e Tecnologie per l'Energia e la Mobilità Sostenibili (STEMS), Consiglio Nazionale delle Ricerche, P. le Tecchio 80, Naples 80125, Italy
[c] Department of Chemical Sciences, University of Naples Federico II, Via Cinthia 4, Naples 80126, Italy

ARTICLE INFO

Keywords:
Hydrogen
Glycerol
Sodium metaborate
Polymer
Biogenic carbon dioxide
Innovative process

ABSTRACT

In the global fight against climate change, the bio-based supply chain represents an interesting solution as it offers the potential to produce high-value-added products and bioenergy through the utilization of waste and by-products. In this work, a new route is proposed for the conversion of bio-based glycerol to H_2/CO_2 and high value-added liquid and solid products. The innovative process used pure or crude glycerol or ethanol-glycerol mixture along with water and sodium metaborate as reagents at 300 °C under discontinuous conditions. The gas stream consists mainly of hydrogen, followed by biogenic CO_2 (31–54 %), CO (4–13 %) and CH_4 in traces. The presence of water in the tested crude glycerol improved the hydrogen selectivity to 55 %. Characterization of the liquid reaction products revealed the synthesis of products such as 1,2-propanediol, propanoic acid, acetic acid, cyclopentenones and cyclic diglycerol. In the solid phase, an aliphatic hydrocarbon resin with oxygenated carbon along the saturated chain and an aromatic cluster were also characterized by NMR, FTIR and TG analyses. Based on these findings, the global reaction route to the general reaction products was proposed.

1. Introduction

Today, the energy and chemical industry is based on the use of fossil fuels, but their massive exploitation use is causing negative environmental impacts. Therefore, there is an urgent need to develop alternative and sustainable methods to meet the growing demand for energy and chemicals [1]. Promising solutions are emerging by an holistic approach which combines valorization of wastes and industrial by-products with the concurrent use of renewable hydrogen as energy source.

Glycerol is a primary by-product of the transesterification reaction, which transforms triglycerides, or vegetable oil, into long-chain mono alkyl esters, or biodiesel. Glycerol makes up around 10 % of the weight (wt) of the biodiesel that is generated [2]. Biodiesel production processes are conducted in the presence of an alcohol, typically methanol or ethanol and a catalyst, usually sodium hydroxide. Consequently, crude glycerol contains impurities, including water, alcohol, soap, inorganic salts, and organic non-glycerol matter and the glycerol amount ranges from 30 to 90 % [3,4].

In 2030, it is estimated that crude glycerol production will be over four billion gallons per year, or 49,882 million liters, according to the Organization for Economic Co-operation and Development (OECD) [3]. The production of crude glycerol from biodiesel has been increasing day-by-day, and this has caused an annual glut in supply, exerting downward price pressure. Brought to today value of about 0.50 USD/L, crude glycerol is effectively sold at a whopping 67 % under the cost pure glycerol (1.50 USD/L) [5,6]. This surplus poses a significant challenge to the growth of the biodiesel industry, making biodiesel economically unviable. Because it is a cheap and readily available feedstock, the use of both crude and purified glycerol is crucial to promoting the use of biodiesel [7].

In this context, contemporary research efforts are aimed at exploring the potential utilization of glycerol as a feedstock, with the overarching goal of producing value-added organic compounds [8,9]. Two well-established reforming processes, steam reforming (SR) and aqueous phase reforming (APR), represent two major routes in hydrogen synthesis from glycerol [10]. Through a variety of reaction pathways, glycerol functions as a precursor for a broad range of industrially

* Corresponding author.
E-mail address: alessandra.dinardo@unina.it (A. Di Nardo).

https://doi.org/10.1016/j.cej.2024.156634

Available online 11 October 2024

significant reactions, including dehydration pathways for acrolein production [11–13] and hydrogenolysis for generating key intermediates like 1,2-propanediol, essential intermediates in polymer and pharmaceutical industrial processes [14–16]. Additionally, glycerol, involved in oligomerization reactions, produces di- and tri-glycerol isomers, used as solvents and intermediates [17–19]. Moreover, the application of glycerol in bioplastics and resins demonstrates the important role it can play in promoting sustainability [20–23].

As for the valorization of waste as a source of materials, sodium metaborate, a solid difficult-to-regenerate by-product in the context of hydrogen storage, is used in a new patented process for the simultaneous production of Cyan Hydrogen and polymers [24]. The process consists of consecutive steps exercised under batch conditions and 300 °C, involving the alternating addition of bio-alcohol and water to an alkali metal salt of metaborate ($YBO_2{\cdot}xH_2O$, where Y represents an alkali metal and x the hydration degrees), a by-product of hydrogen storage process. In a previous work [25], it was reported that the use of ethanol and sodium metaborate for four process steps allows the simultaneous production of hydrogen rich gas (>95 %, v/v), an oligomeric compound with a repetitive carbon pattern $(-CH_2-CH_2-)_n$, and a liquid phase rich in oxygenated organic compounds.

The innovation of this process lies in both the selection of raw materials and the variety of products generated, which allows for the simultaneous production of hydrogen and carbon valorization. The utilization of bio-derived feedstocks fits into the discussed context by operating with inherently CO_2-neutral raw materials. Moreover, the process offers the possibility to reuse metaborate from metal borohydride hydrolysis used for hydrogen storage, since borohydride regeneration is a tedious and uneconomical process [26].

In the proposed work, we aim to evaluate the feasibility and efficiency of the new process by investigating the use of glycerol, chosen as bioderived feedstock for its cost-effectiveness and abundance [27,28]. This choice is not only in line with economic considerations, but also offers environmental benefits by using a by-product of biodiesel production. For these reasons, the article investigates the novel process for transforming bio-based glycerol, which may be in the form of pure, crude, or combined with ethanol, utilizing sodium metaborate at a temperature of 300 °C. Glycerol was tested to investigate the effect of the feedstock on cyan hydrogen production and liquid and polymeric products. Moreover, a mixture of ethanol, pure glycerol and crude glycerol were used as raw materials to assess the effect of the co-presence of the two alcohols on the composition of each phase and to assess the feasibility of using low-cost impure glycerol in this novel process.

2. Material and methods

2.1. Materials

The following reagents were used for the experimental tests: sodium metaborate tetra-hydrate ($NaBO_2{\cdot}4H_2O$, CAS: 10555–76–7, 99.95 % wt), distilled water, ethanol (C_2H_5OH, CAS: 64–17–5, ≥99.8 % wt), and glycerol ($C_3H_8O_3$, CAS: 56–81–5, ≥99.5 % wt). All the reagents were purchased from Sigma-Aldrich and used as received. The composition of the synthesized crude glycerol utilized was 78.0 % wt glycerol, 20.7 % wt water, and 1.3 % wt ethanol [29].

2.2. Experimental setup

The experimental setup was as described in our previous work [24]. Briefly, as reported in the experimental set-up schematization (Fig. 1), a batch reactor vessel with a volume of 450 mL (Parr 4567) was used. The reactor system included a pressure gauge, an internal stirring system, a thermocouple, a liquid sampling valve, a gas release valve, a gas inlet valve, a safety rupture disk, an electric heater, a mixer motor and a temperature, pressure and stirring rate control system (Parr 4848). A pressure transducer attached to the reactor is used to detect the reactor pressure.

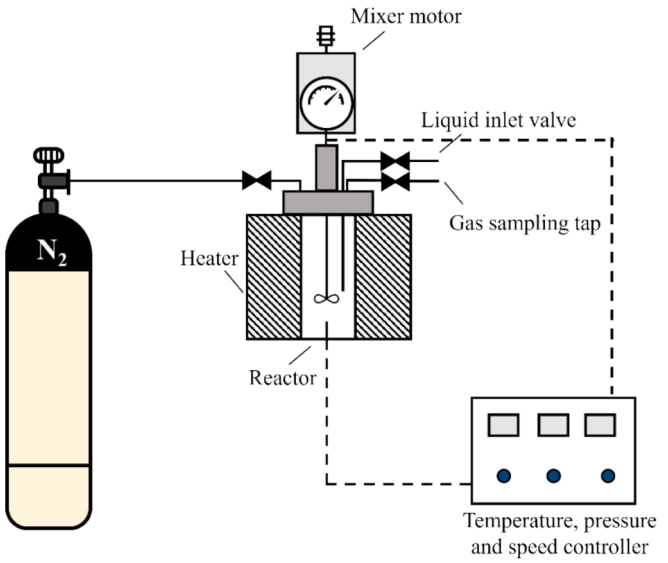

Fig. 1. Schematic representation of the experimental set-up.

2.3. Experimental procedure

The process consists of four sequential reaction steps, schematized in Fig. 2. The operating conditions along with the reagent quantities are presented in Table 1. In the following, the process in the presence of glycerol, crude glycerol or a mixture of ethanol and glycerol as organic feedstock ***(A)*** is described. As detailed in Fig. 2, initially, sodium metaborate ***(B)*** was introduced into the vessel along with organic feedstock ***(A)*** in the first step of the process. Next, water ***(C)*** was added to the system, and the reaction occurred under the same operating conditions as in the first step. More feedstocks ***(A)*** were added in the third steps, with a final water addition in the last step. The reaction system comprised three phases and produced solid, liquid, and gaseous products.

Before the initial experimental step, the reagents were placed into the vessel and a pressure purge inertization (six cycles of inerting from 0.3 to 5.0 barg in N_2) was carried out. After the time of reaction t_r, the system was cooled, and gas was sampled at a temperature of 60 °C and a variable pressure depending on the reaction step (Table S1). Water was introduced into the system through the liquid inlet valve at room temperature, and then after purging, the second phase began. The experiment was subsequently repeated for all steps, following the same procedure as described for the first step. At the end of the process, i.e., the fourth step, the reactor was opened after gas sampling, to recover the final solid–liquid mixture products at room temperature.

85.60 mmol of organic feedstocks ***(A)*** and 14.50 mmol of sodium metaborate $NaBO_2{\cdot}4H_2O$ ***(B)*** were used in each test, maintaining a constant ratio of organic raw material to metaborate at approximately 6. In the case of glycerol (Gly), the organic feedstock consisted of 85.60 mmol of pure glycerol; for the crude glycerol (CruGly), the total amount of moles was divided into 78.0 % wt glycerol, 20.7 % wt water, and 1.3 % wt ethanol [29] while for the ethanol-glycerol mixture (EtOH-Gly), the composition was 50/50. To summarize, molar amounts of each component are reported in Table S2, and the nomenclature employed will be utilized throughout the text to designate the investigated processes.

2.4. Analytical methods

Gas composition was analyzed by Agilent 3000A micro gas

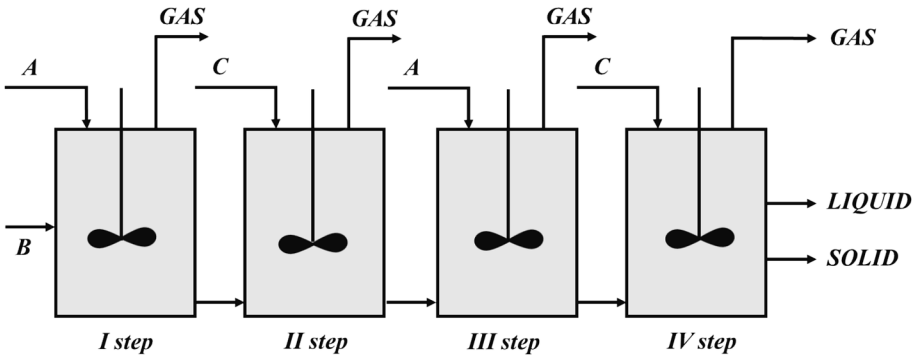

Fig. 2. Block diagram of the process involving four consecutive reaction steps, with alternating organic feedstock **(A)** and water **(C)** added to sodium metaborate **(B)**, in a batch reactor.

Table 1
Operating conditions and molar quantities of process fed reagents.

Operating conditions	
Temperature, T	300 °C
Stirring speed	500 rpm
Initial pressure (N_2), P_{in}	0.3 barg
Time of reaction, t_r	6 h
Gas sampling Temperature, T_{gs}	60 °C
***(A)** Organic feedstock*	85.60 mmol
***(B)** $NaBO_2{\cdot}4H_2O$*	14.50 mmol
***(C)** H_2O*	555.0 mmol

chromatography (microGC) equipped with OV-1, Alumina, PLOT-U and MS5A columns, and a thermal conductivity detector (TCD). The temperatures of the OV-1, Alumina, PLOT U, and MS5A columns were 65, 90, 80, and 100 °C, respectively. Helium was used as the carrier gas for columns OV-1, Alumina, and PLOT U, whereas column MS5A employed argon. Each analysis was repeated five times for each sampling bag analyzed.

The crude reaction product (an immiscible liquid phase and a black solid) was centrifuged (ALC mod. 4222 MK II, Sigma) at 5000 rpm for 5 min, at 25 °C (Scheme 1). The supernatant (S) obtained was lyophilized and the corresponding material was completely solubilized with chloroform (S-$CHCl_3$), ethyl acetate (S-AcOEt), and water (S-H_2O). The precipitate (P) obtained from centrifugation was soluble in chloroform (P-$CHCl_3$). The fractions obtained were analyzed by NMR. The ^1H and ^{13}C NMR spectra were recorded with an NMR spectrometer operated at 400 MHz and 25 °C (Bruker DRX, Bruker Avance) and referenced in ppm to the residual solvent signals ($CDCl_3$, at δ_H 7.26 and δ_C 77.2, or D_2O at δ_H 4.79).

The identification of compounds in bare liquid samples (S) was performed by gas chromatographic analysis implementing a mass spectrometer for the detection (GC–MS) in Agilent HP6890/HP5975 instrument. The samples were diluted in methanol and 1 mL of each solution was injected at 50 °C with separation performed on a DB-624 column with helium as the carrier gas. The oven temperature was programmed to increase from 50 °C at a rate of 5 °C/min to 260 °C, at which it was held for 15 min.

The selectivity was evaluated using the following equation for gas Eq. (1) and liquid Eq. (2) products:

$$\text{Selectivity}_{\text{GAS,i}} = \frac{\text{Mole of i} - \text{species produced}}{\text{Total moles}} \quad (1)$$

$$\text{Selectivity}_{\text{LIQUID,i}} = \frac{\text{Peak Area i} - \text{species produced}}{\text{Total Area}} \quad (2)$$

Performance Index *I* was defined as shown in Eq. (3) to compare the proposed methodology with other hydrogen generation process.

$$\text{I} = \frac{\text{Mole of } H_2 \text{ produced}}{4 \text{ x Moles of Gly inlet}} \quad (3)$$

After separation, the bare solid product (P) of the reaction was washed five times with ethanol. In each cycle, the residue was dispersed in the solvent and sonicated at 59 kHz for 10 min, centrifuged and separated. The resulting solid phase was dried in a vacuum oven at 100 °C overnight.

Chemical bonds of solid products were evaluated through Fourier-transform infrared spectroscopy (FTIR) in a Nexus FTIR spectrometer Nicolet 5700. The FTIR absorption spectra were captured at a spectral resolution of 2 cm^{-1} within the 4000–500 cm^{-1} range.

Thermogravimetric analysis (TGA) was conducted with the TGA/DSC TA Q600SDT instrument, which permits the simultaneous measurement of weight change and differential scanning calorimetry (DSC). TGA analysis was carried out under N_2 and air streams at a heating rate of 10 °C/min up to 1000 °C with platinum pans employed to assess the thermal stability of the substances. Additionally, to identify the degradation of gaseous products, TG-FTIR was conducted in N_2 gas at a heating rate of 10 °C/min, coupling a transfer line and the spectrometry cell to the TG instrument. The cell and transfer line of the TGA/FTIR

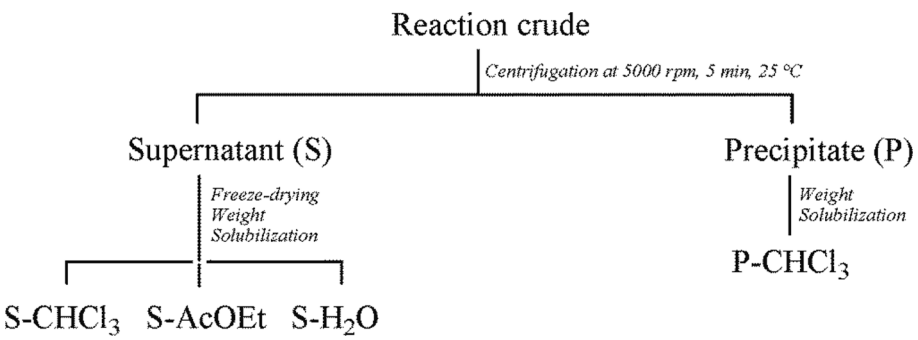

Scheme 1. Fractionation of the reaction crude.

interface were heated and kept at 220 °C. In this way, product gases from samples degradation could not condense. The output of this analysis is a Gram-Schmidt diagram. The HR Nicolet TGA Vapor Phase library of OMNIC software was used to identify the product gases.

X-Ray Diffraction (XRD) analysis was conducted through XRD diffractometer PANalytical X'Pert Pro using Cu Kα radiation (1.5406 Å). The scanning range of 2θ is [5°; 100°] with a step size of 0.013° and a scan step time of 18.87 s.

Elemental analysis of solid residues was carried out with CHN 628 LECO, to measure the percentage content of Carbon (C), Hydrogen (H), and Nitrogen (N) in the samples. Through the results of the thermogravimetric analysis in air and elemental analysis, it was possible to estimate the elemental Oxygen (O) content in % wt by the following equation Eq. (4).

$$O = 100 - C - H - N - \text{Moisture} - \text{Ash} \quad (4)$$

The moisture and ash content were evaluated as the weight loss up to 200 °C and as the percentage of residual weight at 1000 °C during thermogravimetric analysis.

A FEI Inspect Scanning Electron Microscope was used to characterize the microstructure; the microscope is equipped with an energy dispersive X-ray (EDX) probe for the elemental analysis.

3. Results

Experiments were carried out to test the Cyan Hydrogen production process (described in Section 2.2) using three feedstocks: Glycerol (Gly), an equimolar mixture of Ethanol and Glycerol (EtOH-Gly), and Crude Glycerol (CruGly), following the methodology outlined in Section 2.3. The results of the characterization of the gaseous, solid, and liquid products are presented below and the consequent Discussion is reported in Section 4.

3.1. Gas pressure profiles and product volumetric composition

Fig. 3 shows the pressure profiles over time for the different bio-building blocks during the process that consisted of four consecutive steps at 300 °C in a closed vessel. The pressure had an increasing trend during the heating ramp, and then reached the final plateau value, given in Table 2. The pressure profiles were significantly influenced by the organic reagent fed during the I step. The initial phase of the I step is indicative of the reagent evaporation during heating. The differences among the pressure profiles between feeds can be explained by different vapor pressures of the components and their interactions in the process of reaction. The steepest slope was observed for the ethanol and glycerol mixture (orange line, Fig. 3), where ethanol has the lowest boiling temperature in comparison with pure glycerol and crude glycerol (green and light blue lines, Fig. 3). In contrast, pure glycerol with its higher boiling point had a more gradual pressure increase. Crude glycerol, containing both water and ethanol along with glycerol, showed an intermediate behavior reflecting the combined effects of its components boiling points. During the subsequent steps, the pressure curves overlapped during the heating ramp but differed in the final pressure value reached (Table 2).

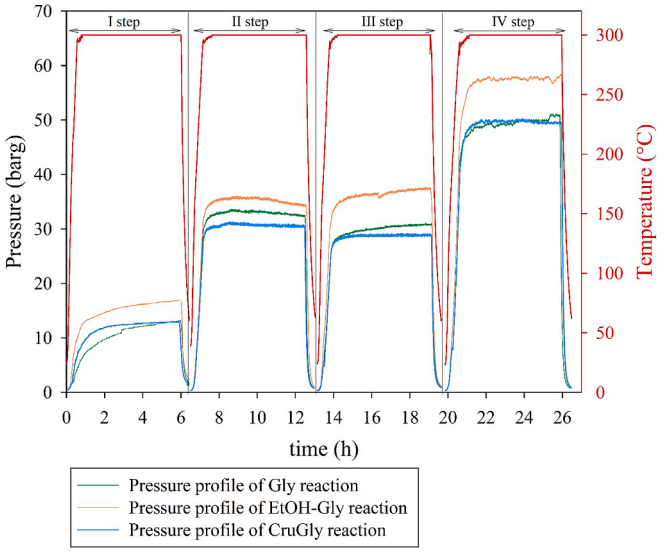

Fig. 3. Pressure and temperature profiles during the process by feeding glycerol (Gly), mixture of ethanol and glycerol (EtOH-Gly), and crude glycerol (CruGly). The maximum standard deviation s was ± 1.4.

At the end of each step, the gas was cooled to 60 °C, sampled and analyzed by means of microGC; the gas sampling pressure is given in Table S1. Table 2 shows the volumetric gas composition with standard deviation as obtained by feeding Gly, EtOH-Gly, and CruGly at different process steps. The results obtained by feeding ethanol are also given for the sake of comparison [25]. The main gaseous products are hydrogen (H_2), carbon dioxide (CO_2), carbon monoxide (CO), methane (CH_4), and higher hydrocarbons ranging from C2 to C6.

The volumetric composition of H_2 obtained during the various process steps from the tested feedstocks was in the range of 38–60 %, followed by CO_2 in the range of 31–54 %, CO between 4–13 %, and CH_4 between 0.0–0.5 %. Gaseous hydrocarbons with carbon chains ranging from C2 to C6 were also found in small quantities (0.9–9.4 %) as glycerol cracking products [30].

The high hydrogen composition (>95 %) observed with pure ethanol [25] can be addressed to its simpler molecular structure, which results in the production of fewer byproducts compared to glycerol. Conversely, glycerol gives rise to a greater number of side reactions and a lower degree of hydrogen purity, due to the formation of additional gases such as CO_2, CO, CH_4 and light hydrocarbons.

The simultaneous change in temperature and consequently in pressure in the closed vessel over time resulted in the formation of liquid and gaseous mixtures of varying composition. During the heating and the isothermal phase, the amount of feedstock passing into the gas phase changed over time. The formation of liquid and gaseous mixtures with time-varying composition (and fed ratios), occurring in parallel simultaneously led to different amounts of hydrogen production as the starting reagent changed. In addition, at a temperature of 300 °C, sodium metaborate completely lost its four moles of structural water [31], thus becoming part of the gaseous mixture. The formation of a two-phase reaction system suggests that both gaseous steam reforming and aqueous phase reforming reactions occur in parallel, with different H_2O/Alcohol ratios changing with time.

Pure ethanol passed more easily into the gas phase during heating, accompanied by the structural water of sodium metaborate and the water fed during the II step, leading to a major increase hydrogen production. The process in the presence of glycerol led to the lowest average hydrogen production during the steps (43.5 %), whereas in the presence of ethanol-glycerol mixture and crude glycerol, an average value close to 50 % was reached. Glycerol, in a mixture or pure form, led to lower hydrogen production suggesting that its higher evaporation temperature disfavored the vapor phase reaction.

Besides ethanol, reported in the article for comparison, among the bio-building blocks analyzed, crude glycerol appears to be the most promising option, resulting in more hydrogen production and less CO_2. This suggests that the presence of water may favor hydrogen production. However, the highest amount of formed heavier hydrocarbons was registered in the case of crude glycerol when water was added as a reactant during the I step. It is also interesting to note that for each feedstock tested, the greatest CO production occurred during the first process step, which was then attenuated in subsequent steps, indicating how the presence of water reduced its production.

Table 2
Final pressure and volumetric gas composition for the reaction steps in presence of glycerol (Gly), an equimolar mixture of ethanol and glycerol (EtOH-Gly), and crude glycerol (CruGly) obtained from microGC analysis with standard deviation. In Table are reported the results in presence of ethanol (EtOH) from our previous work [25].

Organic feedstock	Process step	Volumetric Gas Composition (%)					Pressure (barg)
		H_2	CO_2	CO	CH_4	C2-C6	
EtOH Ref. [25]	I	94.83 ± 0.27	1.67 ± 0.24	0.00 ± 0.00	0.00 ± 0.00	3.47 ± 0.06	13.8
	II	93.48 ± 0.21	5.7 ± 0.16	0.00 ± 0.00	0.00 ± 0.00	0.102 ± 0.07	39.5
	III	98.56 ± 0.05	1.09 ± 0.05	0.00 ± 0.00	0.00 ± 0.00	0.20 ± 0.03	46.9
	IV	95.2 ± 0.04	2.54 ± 0.08	0.00 ± 0.00	0.00 ± 0.00	0.70 ± 0.05	52.1
	Average	***95.52***	***2.75***	***0***	***0***	***1.12***	
Gly	I	47.64 ± 0.04	38.30 ± 0.16	12.30 ± 1.09	0.28 ± 0.41	1.72 ± 2.37	13.2
	II	42.75 ± 0.08	48.90 ± 0.02	6.68 ± 0.83	0.00 ± 0.21	2.84 ± 3.10	32.4
	III	45.45 ± 0.09	43.13 ± 0.10	9.83 ± 0.00	0.47 ± 0.00	1.99 ± 1.27	30.8
	IV	38.19 ± 0.07	52.17 ± 0.02	6.61 ± 0.65	0.30 ± 0.00	3.88 ± 1.41	50.9
	Average	***43.50***	***45.62***	***8.85***	***0.26***	***2.60***	
EtOH-Gly	I	47.11 ± 0.67	40.81 ± 0.11	11.22 ± 0.01	0.00 ± 0.01	0.92 ± 0.36	20
	II	36.82 ± 0.02	53.55 ± 0.01	4.16 ± 0.00	0.00 ± 0.00	5.73 ± 0.14	34.1
	III	50.5 ± 0.08	40.11 ± 0.05	5.66 ± 0.01	0.00 ± 0.01	3.81 ± 0.09	36.3
	IV	59.46 ± 0.04	31.57 ± 0.03	4.73 ± 0.00	0.00 ± 0.00	4.26 ± 0.12	58.2
	Average	***48.47***	***41.51***	***6.44***	***0***	***3.68***	
CruGly	I	53.02 ± 0.38	33.15 ± 0.54	11.00 ± 0.04	0.20 ± 0.04	2.72 ± 0.52	13
	II	46.48 ± 0.66	38.59 ± 0.48	5.60 ± 0.02	0.12 ± 0.02	9.41 ± 1.25	30.5
	III	48.03 ± 0.97	44.37 ± 0.86	5.67 ± 0.03	0.16 ± 0.03	2.18 ± 2.10	28.8
	IV	55.86 ± 0.75	34.23 ± 0.53	3.80 ± 0.02	0.18 ± 0.02	6.32 ± 1.26	49.3
	Average	***50.85***	***37.59***	***6.52***	***0.17***	***5.16***	

3.2. Liquid products

3.2.1. NMR analysis on the reaction raw material

The S-H_2O fraction was the most abundant and the NMR analysis indicated the presence almost exclusively of glycerol. In addition, the S-H_2O fraction showed the presence of slightly polar material, with the prevalence of signals of alkyl protons and only the minimal presence of protons of oxygenated and aromatic compounds. The S-AcOEt fraction still showed glycerol residues but also signals between 0 and 2.5 ppm, owing to the presence of material containing alkyl residues, and signals between 3.0 and 5.0 ppm, owing to the presence of protons geminal to oxygenated carbons. The presence of aromatic protons was almost negligible (~5%). The S-$CHCl_3$ fraction showed exclusively the presence of oxygenated alkyl compounds as well as a good presence of aromatic signals (~10 %). This hypothesis was confirmed by the IR spectrum which showed a band centred around 3300 cm^{-1} indicating the presence of hydroxyl groups. The presence of oxygenated alkyl and aromatic signals become more pronounced as the apolarity of the solvent increased, suggesting the presence of alkyl chains with oxygen along the chain that do not impart polarity to the compound.

3.2.2. Identification of species through GC–MS analysis

Several compounds were identified by GC–MS analysis. The characterization indicated that the liquid products from the reaction of glycerol, ethanol and glycerol, and crude glycerol were mainly comprised of acetic acid (*m/z* 60), three-carbon constituents dominated by propanoic acid and propylene glycol, also known as 1,2-propanediol (*m/z* 76), and (C5-C6) compounds such as cyclopentenone mono-, bi- and tri-substituted, and cyclic diglycerol, as listed in Table 3. Selectivity and a possible reaction pathway are presented in the discussion section (Section 4).

Table 3
Compounds identified by GC–MS analysis on liquid products and relative retention time.

GC–MS characterization	
RT (min)	**Compounds**
5.780	2-Butanone
7.651	Acetic acid
10.806	Acetoin
11.253	Propanoic acid
13.293	1,2-Propanediol
13.435	Cyclopentanone
14.249	Ethylboronic acid
14.747	2-Methyl-2-propenoic acid
15.253	2-Methyl-cyclopentanone
15.508	2-Cyclopenten-1-one
17.948	2-Methyl-2-cyclopenten-1-one
18.897	3,4-Dimethyl-2-cyclopenten-1-one
20.857	3-Methyl-2-cyclopenten-1-one
22.709	Phenol
23.062	2,3-Dimethyl-2-cyclopenten-1-one
24.602	Glycerol
24.374	1,2,3,4-Butanetetrol
24.587	2-Methylphenol
31.159	Bis(2,5-hydroxymethyl)dioxane
32.066	Bis(2,6-hydroxymethyl)dioxane
36.114	2,3-Dihydro-1,4-benzodioxin-2-methanol

3.3. Chemical structure and properties of solid products

3.3.1. Functional groups and NMR characterization

Fig. 4 shows the comparison of the FTIR spectra of Gly, EtOH-Gly, and CruGly reaction products denoted by green, orange, and light blue lines, respectively. The band assignments are listed in Table S3. There is considerable overlap between the spectra although there are some differences in peak positions and intensity. The broad band around 3500–3400 cm^{-1} corresponds to stretching vibration (ν) modes of the OH group, ν(OH), and the presence of aliphatic carbons in the 3000–2800 and 1480–1370 cm^{-1} ranges is highlighted in grey in Fig. 4, consistent with previous research [32]. Specifically, absorptions at 2955, 2925, and 2868 cm^{-1} were ascribed to antisymmetric and symmetric stretching vibrations (ν_{as} and ν_s), ν_{as}(C-H_3), ν_{as}(C-H_2), and ν_s(C-H_2), respectively. Furthermore, features associated with aliphatic hydrocarbon bonds, such as bending (δ) of CH_2 moiety, δ(C-H_2) at 1453 cm^{-1} and δ(C-H_3) at 1375 cm^{-1}, suggested the presence of slight branching of the hydrocarbon chains [33]. In addition, evidence of aromatic structural moieties was inferred from the average intensity of absorption bands spanning the range 3050–3000, 1620–1590, and 900–700 cm^{-1}. The stretching of the ring C-H bonds, where the hydrogens are bound to sp^2 carbons, was discernible above 3000 cm^{-1}.

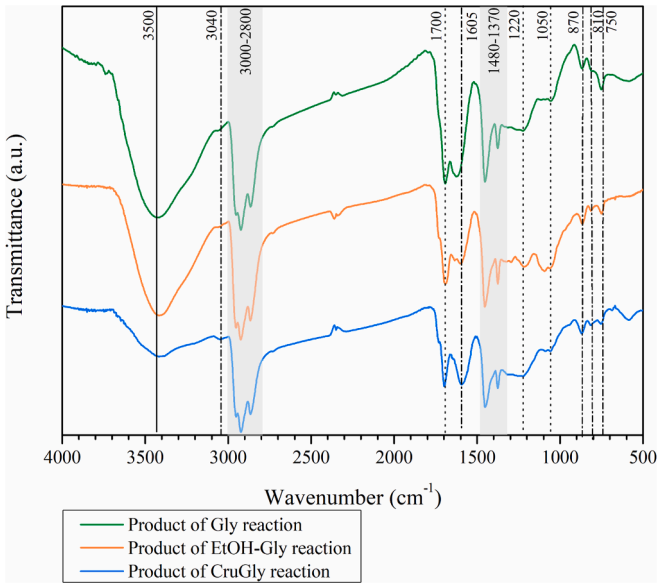

Fig. 4. FTIR spectra of solid reaction products in presence of glycerol (Gly), an equimolar mixture of ethanol and glycerol (EtOH-Gly), and crude glycerol (CruGly).

Moreover, out-of-plane C-H bending vibrations of aromatic compounds, with three peaks of low intensity at 870, 812, and 750 cm^{-1} were observed, alongside ν(C=C) ring modes at 1605 cm^{-1} [34,35]. Oxygen-containing functional groups, specifically carbonyl (C=O) at 1700 cm^{-1}, C-O at 1220 cm^{-1}, and ether (C-O-C) at 1110 and 1030 cm^{-1} were identified in all the spectra [36]. Notably, the typical absorption region of carbonyl is 1740–1730 cm^{-1}, but conjugation with the aromatic ring can induce a shift towards the lower absorption region of 1710–1690 cm^{-1} [37].

The spectra were identified as belonging to an aromatic hydrocarbon resin found in the Hummel Polymer library using the OMNIC software with a match of 65 %. This identification was then confirmed by comparing it with literature spectra [34,35]. As previously mentioned, peak assignments (as summarized in Table S3) were consistent across all spectra.

In addition, a preliminary NMR characterization was performed on the raw solid and the precipitate (P) obtained from centrifugation was completely soluble in chloroform (P-$CHCl_3$). The NMR data indicated the presence of a higher intensity zone related to slightly polar alkyl compounds and only traces of oxygenated and/or aromatic compounds. Therefore, this evidence confirmed what was shown by the IR spectra, i.e. the presence of carbonyl groups with absorption bands around 1700 cm^{-1}, alkyl groups (3000–2800 and 1480–1370 cm^{-1}) with higher intensity, and aromatic compounds with absorption bands at 3040 and between 900–700 cm^{-1}. The XRD (Fig. S1) diffraction patterns exhibited a broad halo in the range 20-45°, confirming the presence of an amorphous phase and disappearance of the crystalline structure of sodium metaborate [38]. The solid compound was therefore extremely insoluble in the aqueous phase and strongly apolar and amorphous, indicating a heterogeneous mixture. Future analyses will allow the chemical structure of the polymer to be identified.

3.3.1.1. Elemental analysis. Elemental analysis of solid products is presented in Table 4. Carbon was the most abundant element in all samples. The hydrogen content was 7.10 % wt in the case of Gly product, and 7.29 % wt and 6.65 % wt in the EtOH-Gly and CruGly products, respectively. The oxygen content, estimated as described in Section 2.4, was found to be consistent across all process products at approximately 10 % wt. As a measure of the degree of hydrogenation (H/C) and oxygenation (O/C) of the samples, atomic molar ratios were evaluated

Table 4
Organic Element Content (%wt) and H/C and O/C molar ratios.

	Elemental Analysis					
Organic feedstock	C	H	O	Inorganic content	H/C	O/C
Gly	74.22	7.10	10.68	8.00	1.15	0.11
EtOH-Gly	77.18	7.29	10.15	5.38	1.13	0.10
CruGly	73.94	6.65	n.a.	n.a.	1.08	n.a.

(Table 4). The products showed a degree of hydrogenation between 1.08 and 1.15, alongside a low degree of oxygenation of 0.10. Typically, H/C and O/C atomic ratios represent the degree of aromaticity and the polarity of a polymer. An increase in the H/C ratio is an indication of a high degree of aromaticity, while a high O/C ratio is an indication of a high polarity [39,40]. The H/C ratio decreased from the starting glycerol to the reaction solid product, indicating a dehydrogenation reaction as confirmed by gas analysis. Notably, carbon constituted the highest percentage among the elements analyzed, and the H/C molar ratios suggested a degree of hydrogenation intermediate between aliphatic and aromatic polymers typical [41,42]. In addition, the decrease in the O/C ratio indicates the decrease in compost polarity, as confirmed by NMR and the evolution in the gas phase of CO and CO_2.

By combining the results of FTIR, NMR and ultimate analyses, the solid product chemical structure is mainly composed of a carbon and hydrogen chain, with oxygen as the heteroatom. This is in line with the FTIR spectra (Fig. 4) evidencing large peak intensities of aliphatic carbons. Oxygen is primarily present in terminal carbonyl groups or in conjunction with carbon atom alongside the chains [41,43]. In addition, the intensity of the aromatic carbon group peak is low, resulting in a possible chemical structure consisting of an aromatic cluster core with long alkyl chains with oxygen as the heteroatom. Future detailed analysis could give the chemical structure of the polymer.

3.3.1.2. Thermal stability. Characteristic parameters of TG and DSC analysis at a heating rate of 10 °C/min in air of the Gly and EtOH-Gly products (Fig. S2(a,b)) are reported in Table 5. The oxidative degradation of glycerol reaction solid product (Fig. S2a) can be divided into different stages, highlighted by the change in slope of the thermogravimetric curve and from the distinct exothermic peaks observed in DSC spectra. In particular, the first stage up to 200 °C represented the loss of absorbed water, while the ranges 280–430 °C and 430–540 °C were due to the thermal degradation of organic moieties [44]. The ethanol-glycerol mixture product exhibited an additional degradation step (Fig. S2b) compared to the glycerol reaction product. The final and additional degradation stage occurred at higher temperatures between 530–560 °C. The thermal stability of the product obtained in the presence of glycerol was higher than that of the product obtained in the presence of a mixture of ethanol and glycerol, as evidenced by the higher temperatures at the beginning and end of degradation (see Table 5). In fact, since the decomposition temperature range ($T_{ON\text{-}SET}$-$T_{OFF\text{-}SET}$) for the EtOH-Gly product was higher, it can be deduced that the organic species that decomposed were of a higher molecular weight.

Pyrolysis and high-temperature stability were investigated and compared via TG analysis in N_2 atmosphere (Fig. 5). As highlighted in Fig. 5a, the reaction products with Gly and EtOH-Gly showed two significant degradation steps (at temperatures above 200 °C). In particular, the maximum conversion rate temperatures for the Gly product were estimated to be 360 and 440 °C, higher than the maximum temperature for the EtOH-Gly product, 240 and 420 °C, respectively. In contrast, the reaction product with crude glycerol showed a different behavior from the other products. The thermogravimetric curve displayed a one-step degradation with a maximum temperature of 440 °C. Interestingly, this product was the most thermally stable with a $T_{ON\text{-}SET}$ close to 400 °C. At temperatures above 600 °C, the crude glycerol product continued to degrade at a faster rate than the other products, i.e., −0.04

Table 5
Characteristic parameters of thermal degradation of solid products under Air and N_2 atmosphere.

		TG Analysis					
	Organic feedstock	Decomposition temperature range (°C)	Weight loss (%)	T_{MAX} (°C)	T_{ON-SET} (°C)	$T_{OFF-SET}$ (°C)	Q (KJ/g)
Air	***Gly***	285–435	32	337	323	542	29
		435–540	64	480			
	EtOH-Gly	205–384	16	335	273	580	18.7
		385–530	59	490			
		530–560	19	532			
	CruGly	n.a.	n.a.	n.a.	n.a.	n.a.	n.a.
N_2	***Gly***	315–415	18	360	321	n.a.	n.a.
		415–490	15	440			
	EtOH-Gly	220–390	29	240	212	n.a	n.a.
		390–490	23	420			
	CruGly	380–520	29	440	389	n.a.	n.a.

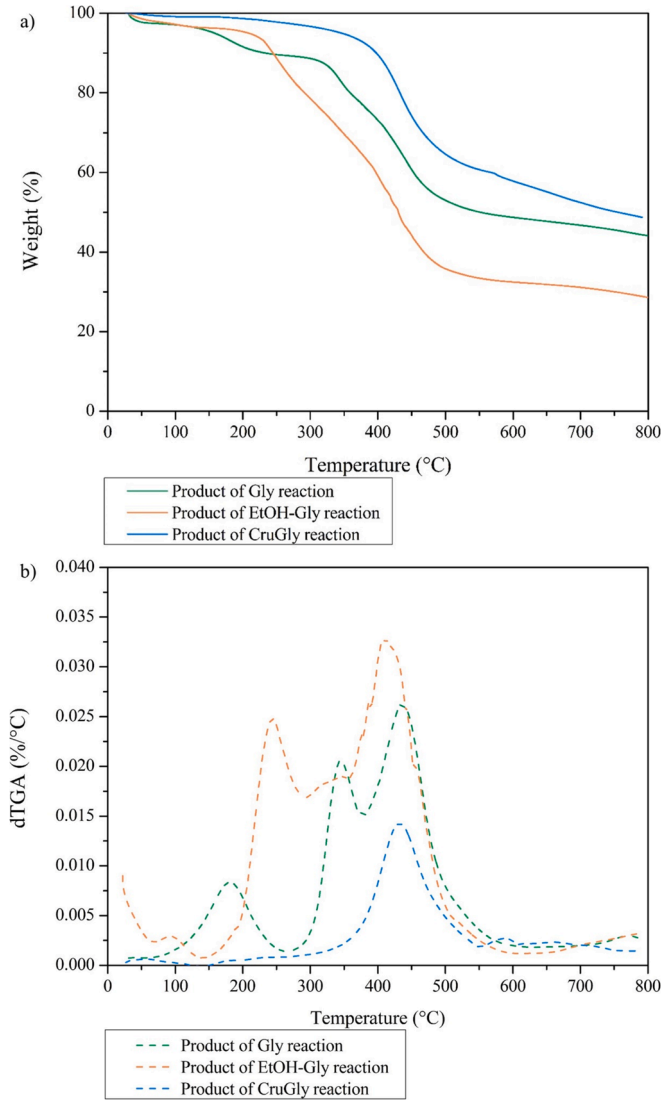

Fig. 5. TG (a) and dTG (b) curves of Gly, EtOH-Gly and CruGly reaction products at 10 °C/min in N_2 atmosphere.

%/°C. Furthermore, as also shown in Table 5, none of the curves reached a plateau, indicating that the degradation did not stop at 800 °C.

The absorption spectra of the gases released during TG at the significant temperatures of 220, 450, and 670 °C are shown in Fig. 6. Firstly, the yellow spectrum collected at 200 °C did not show any significant absorption peaks. Instead, the organic compound pyrolysis was

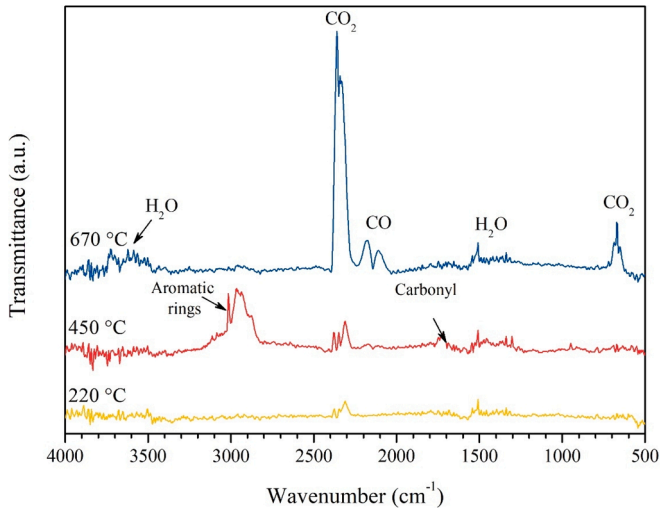

Fig. 6. FTIR spectra of volatiles at different temperature evolved during the TG analysis of CruGly product at 10 °C/min in N_2 atmosphere.

concentrated across a narrow temperature range, in which at 450 °C the highest characteristic absorption peak was observed (red spectrum). Narrow and intense peaks were appreciated in the 3100–3000 cm^{-1} and 1600–1500 cm^{-1} ranges, attributed to the aromatic rings, and intense and defined peaks were observed in the 3000–2800 cm^{-1} range, related to the stretching of CH_2 and CH_3 bonds. The distinct peak at about 1720 cm^{-1} was assigned to carbonyl stretching. During the degradation phase, peak located at 2180 and 2110 cm^{-1} and attributed to CO appeared with a weak intensity. Finally, the blue spectrum reported in Fig. 6 collected at 670 °C, during the second thermal degradation phase, showed continuous production of CO (2180 and 2110 cm^{-1}) and CO_2 (doublet peak at 2360 and 2310 cm^{-1} and peak at 650 cm^{-1}).

The thermal degradation profiles show distinct trends for the three products, suggesting different thermal stabilities. The presence of multiple degradation stages can be attributed to the heterogeneous nature of polymeric products, which were composed of aliphatic, aromatic and oxygenated fractions, as revealed by FTIR and NMR analyses. Typically, the first degradation peak is associated with the decomposition of aliphatic groups and oxygen bonded carbons, while the higher temperature range corresponds to the breakdown of aromatic moieties and carboxyl groups [45,46]. From the FTIR spectra, and as confirmed by NMR, the polymeric product of CruGly reaction showed a higher intensity of the aromatic fraction (peak at 1605 cm^{-1}, Fig. 6). This structural feature explains the higher thermal stability of this polymer compared to those derived from Gly and EtOH-Gly. Additionally, the possible formation of higher molecular weight products is supported by the increased production of gaseous hydrocarbons (C2-C6) during the

reaction (Table 2).

3.3.1.3. Morphological Observations. Fig. 7 presents high-resolution SEM images of the Gly and EtOH-Gly solid products, giving information about their morphologies and surface properties. Fig. 7a exhibits a complex, heterogeneous morphology represented by an agglomeration of irregularly shaped particles and spheres. SEM-EDX (Fig. S3) showed a uniform dispersion of carbon, underling the prevalence of the organic matrix as confirmed by the superficial elemental distribution in weight reported in Table 6. The localized concentration of oxygen suggested areas rich in oxidized carbon along the chemical structure, present as carboxyl moieties in the sample, in accordance with FTIR spectra which evidence a band around 1700 cm^{-1} (Fig. 4), typical of carbonyl groups, and the presence of oxygen itself evidenced by EDX. Furthermore, it is important to point out that the spheres and protrusions may not be mappable due to the optical angle. The EtOH-Gly product (Fig. 7b) exhibited a more uniform morphology with predominantly flake-like structures that were less compact with high carbon content (Fig. S4). The oxygen and sodium distributions appeared localized suggesting the presence of unconverted sodium metaborate encapsulated in the resin matrix. The uniformity of the sample, both on the surface and in bulk can be seen from the results of the elemental analysis (Table 4) and the EDX (Table 6). The weight percentages of carbon composition for both analyses are within 70–80 %, hence indicating good homogeneity within the bulk of the sample.

Table 6
Atomic superficial distribution (%wt) of C, O, Na for Gly and EtOH-Gly products by EDX.

Organic feedstock	EDX (%wt) C	O	Na
Gly	76.80	21.4	1.9
EtOH-Gly	71.10	24.6	4.30

3.4. Reaction pathway

Based on the compounds found in the analysis and the operating conditions adopted, a reaction pathway was developed and depicted in Fig. 8. In the reaction scheme, starting from glycerol, the gaseous, liquid, and solid products are denoted by green, blue and red colors, respectively.

The proposed reaction scheme entails a series of cascading reactions facilitated by the in-situ generated H_2. During the process, liquid and gaseous mixtures of glycerol and water of varying composition are generated. Subsequently, water may engage in a reaction with glycerol via APR or SR pathways (Fig. 8, pathway 1), yielding H_2, CO, CO_2, methane, and low-chain derivatives (C_2–C_3) in the gas phase at 300 °C [47].

3.4.1. Direct glycerol dehydration route (pathway 2)

As a starting point, glycerol can undergo dehydration at a reaction temperature of 300 °C, resulting in the formation of water and acetol (Fig. 8, pathway 2) [48,49]. Additionally, considering the presence of sodium metaborate in the reaction system, as reported by Su et al. [50], the B-OH sites could serve as acidic sites for polyols dehydration enhancing the production of acetol from glycerol. It is also noteworthy that sodium metaborate, when reacted with water, forms the tetrahydroxyborate anion $B(OH)_4^-$ [51], which can function as an Arrhenius base, releasing an HO^- group and forming boric acid $B(OH)_3$. Glycerol can then act as a Lewis base, coordinating with the corresponding acid sites of $B(OH)_3$ to form a complex [52]. This complex then dehydrates to form the corresponding enol intermediate, which subsequently undergoes a ketoenol tautomerism reaction to yield the acetol [53]. Notably, acetol was not found in the liquid products, presumably due to its potential consumption via reaction with the in-situ generated H_2. In fact, three parallel reactions can occur starting from acetol, leading to the observed products in the GC–MS analysis, i.e. 1,2-propanediol, acetic acid, and cyclopentenone derivatives (pathways 2a, 2b and 2c).

The reaction pathway from acetol results in the formation of acetic acid (pathway 2a), which is commonly documented in the literature as one of the main liquid products of the SR and APR reaction of glycerol [54–56]. Cortright et al.[57] reported the production of acetic acid during the APR of glycerol at a temperature of about 300 °C. Pompeo et al. [58] also proposed a more detailed reaction pathway for H_2 production by SR of glycerol, in which acetic acid formation arises from acetol hydration-dehydrogenation.

1,2-Propanediol can be produced by acetol hydrodeoxygenation reactions at a reaction temperature of 300 °C (pathway 2b) in agreement with Główka et al. [59] and Akiyama et al. [60]. The absence of other by-products, such as acrolein, commonly encountered in glycerol dehydration, suggests extensive in-situ hydrogen generation pivotal to the hydrodeoxygenation process, facilitating the formation of 1,2-propanediol and subsequent production of propanoic acid trough acrylic acid hydrogenation [61].

In addition to the production of 1,2-propanediol in the presence of in-situ hydrogen, and the production of acetic acid from acetol, a third parallel reaction pathway starting from acetol is possible, as illustrated in pathway 2c (Fig. 8). According to Zhou et al. [62], acetol may undergo tautomerization reactions followed by cross-aldol condensation reactions facilitated by H_2, culminating in the formation of 2,5-hexanedione. First, enolates are formed from tautomerization as intermediate products that then, via aldolic condensation, form 3,5-dihydroxy-4-

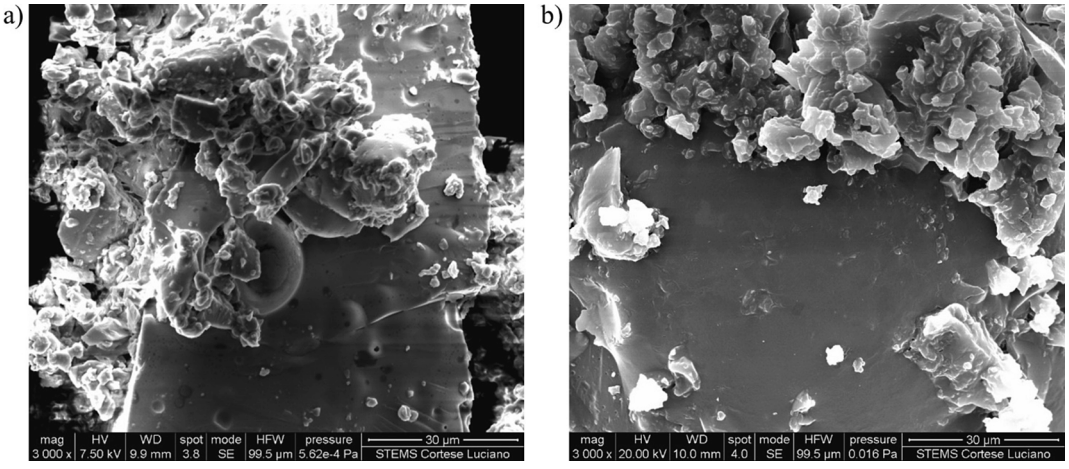

Fig. 7. SEM images of a) glycerol and b) ethanol and glycerol solid reaction products.

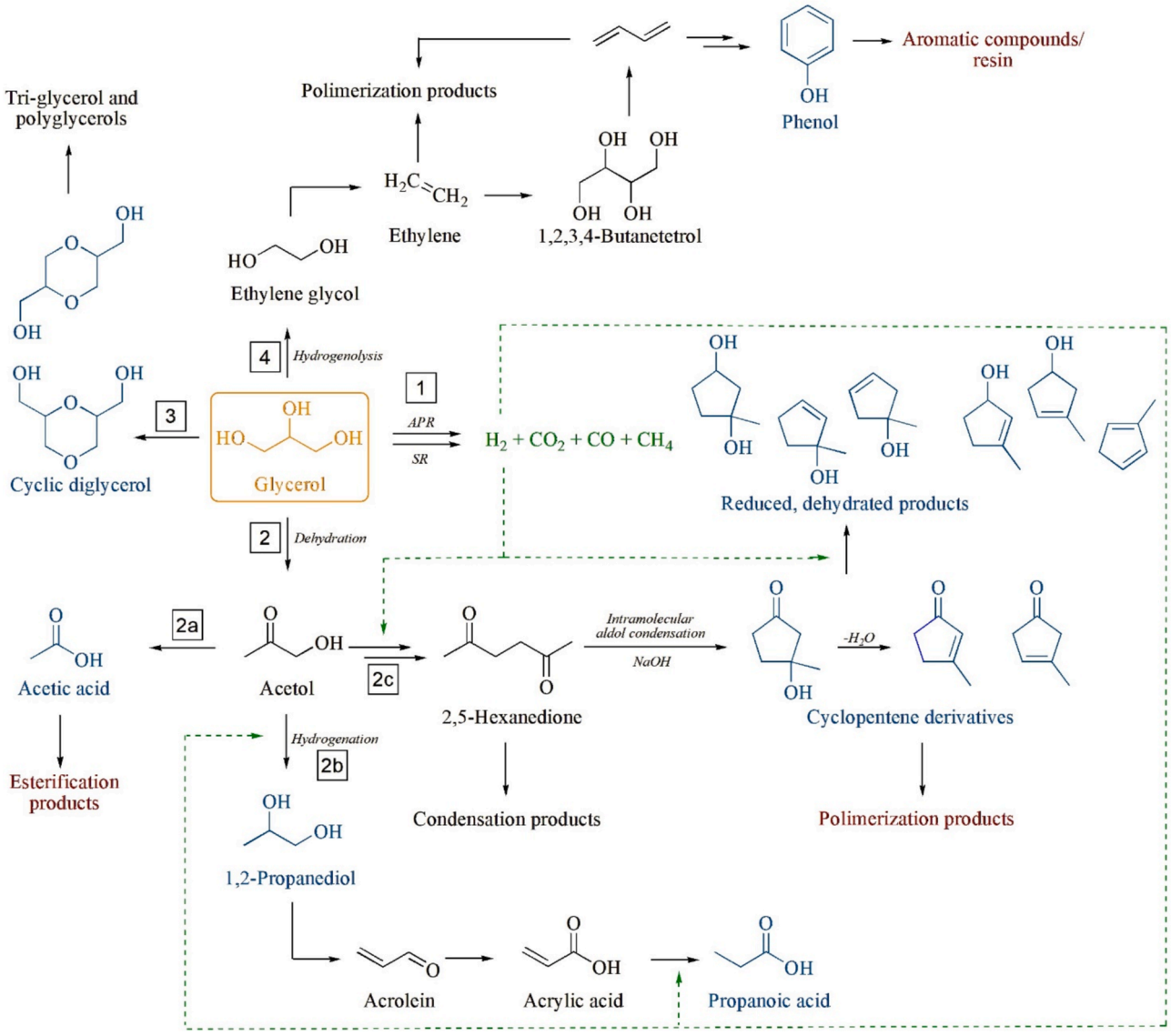

Fig. 8. Reaction pathway in the presence of glycerol and sodium metaborate during the analyzed process. Intermediates and reaction products detected by analysis are colored in green for the gas phase, blue for the liquid phase and red for the solid phase. (For interpretation of the references to colour in this figure legend, the reader is referred to the web version of this article.)

methylpent-3-en-2-one (3,5-DH) and (Z)-1,5-dihydroxy-4-methylpent-3-en-2-one (1,5-DH). The latter, in the presence of hydrogen, forms 2,5-hexanedione via hydrodeoxygenation [63]. Subsequently, 2,5-hexanedione can undergo intramolecular aldol condensation to form cyclic ketonic compounds, such as 2-methyl-2-cyclopenten-1-one and 3-methyl-2-cyclopenten-1-one detected by GC–MS under the investigated operating conditions [64,65]. Intramolecular aldol condensation is a significant method for establishing carbon–carbon bonds in organic compounds with ring structures and involves the formation of a key enolate intermediate through the activation of a basic catalyst [66]. The reaction can be catalyzed by the presence of NaOH [67], which is stable in the operating conditions of the sodium metaborate-water mixture [68]. Finally, cyclopentenones can be reduced in the presence of hydrogen to cyclic pentanones or they can undergo further condensation and polymerization. The aldol condensation reactions may also be intermolecular and involve cyclopentanones, cyclopentenones, their mixtures and/or their derivatives [69]. This would result in the formation of still-reactive products with a higher molecular weight, which could give rise to new reactions to form insoluble amorphous material such as that obtained in the experiments, the cycle of reactions would end with.

As stated in Section 3.3, the solid polymer product appears to be amorphous and heterogeneous and is composed of alkyl, aromatic and carbonyl groups, thus indicating the formation of an aliphatic hydrocarbon resin with oxygenated carbon along the saturated chain and an aromatic cluster. The oxygenated alkyl moiety in the liquid could therefore be the precursor to the precipitated solid phase. Within the reaction scheme, it is possible to highlight different pathways leading to the polymerization product. A polymerization reaction can be obtained from the reaction of glycerol and carboxylic acid, such as acetic acid or propanoic acid, or with oxidized glycerol itself, forming the glycerol polyesters [70,71]. These chains can then be further modified by reacting with polyalcohol or aromatic compounds to form the hybrid resin. It is important to note that during the process, a range of alcohols, including diols, triols, and even polyalcohols, as well as carbonyl and/or carbonyl compounds, are present simultaneously. This could potentially lead to the formation of hemiacetal or acetal compounds, which are not depicted in Fig. 8. It is possible that these compounds will decompose or undergo further inter- and intramolecular reactions, given that they could react with carboxylic and/or dicarboxylic acids. In any case, this

would contribute to the formation of a polymeric material, which is heterogeneous both structurally and in terms of molecular weight distribution.

3.4.2. Glycerol self-etherification reaction (pathway 3)

Glycerol self-etherification reaction occurred concurrently with the cascade reactions mentioned above, leading to the production of cyclic ethers. Self-etherification reaction involves the oligomerization of glycerol to create short-chain oligomers, known as di- and tri-glycerol, or long-chain oligomers, known as polyglycerols. Through condensation reactions, a water molecule is eliminated, and two glycerol molecules combine to form a diglycerol molecule. Diglycerol molecules can take on cyclic, branched, or linear configurations [72,73]. It is possible for these compounds to react with the tetrahydroxyborate anion $B(OH)_4^-$ via the hydroxyl functional groups, not necessarily proximal, and therefore promote cross-linking through the formation of hydrogen and/or covalent bonds [74].

3.4.3. Hydrogenolysis of glycerol (pathway 4)

Ethylene glycol can be generated through hydrogenolysis of glycerol [75–77], and consequently dehydration generates ethylene [78]. Ethylene could be the precursor for the formation of saturated, linear, high-molecular-weight hydrocarbons or it may undergo intermolecular cycloaddition reactions, to form aromatic compounds such as phenol, which is also identified in Table 3 [79,80]. Phenol or analogous compounds could yield the corresponding hydroxylated derivatives, which are then conducive to subsequent oxidation and polymerisation reactions [81].

4. Discussion

As elucidated in Section 3.1, the gaseous products primarily consisted of H_2 and CO_2, with CO, CH_4 and traces of higher hydrocarbons also detected. Within the liquid phase (Section 3.2), identification through GC–MS analysis primarily revealed 1,2-propanediol, ketones, and cyclic ethers. Finally, the solid product consisted of an aliphatic hydrocarbon resin with oxygenated carbon along the saturated chain and an aromatic cluster.

Fig. 9 illustrates the selectivity in the gas phase (a) and in the liquid phase (b) for the different organic feedstock analyzed. As depicted in Fig. 9a, the selectivity towards hydrogen and carbonaceous gaseous products appeared to be minimally affected by the starting reagent. However, the enhanced selectivity towards hydrogen was facilitated by the presence of water in the case of crude glycerol. Furthermore, it is noteworthy that in the case of crude glycerol as a bio-based building block, the initial mole of alcohol fed is smaller than in the other two

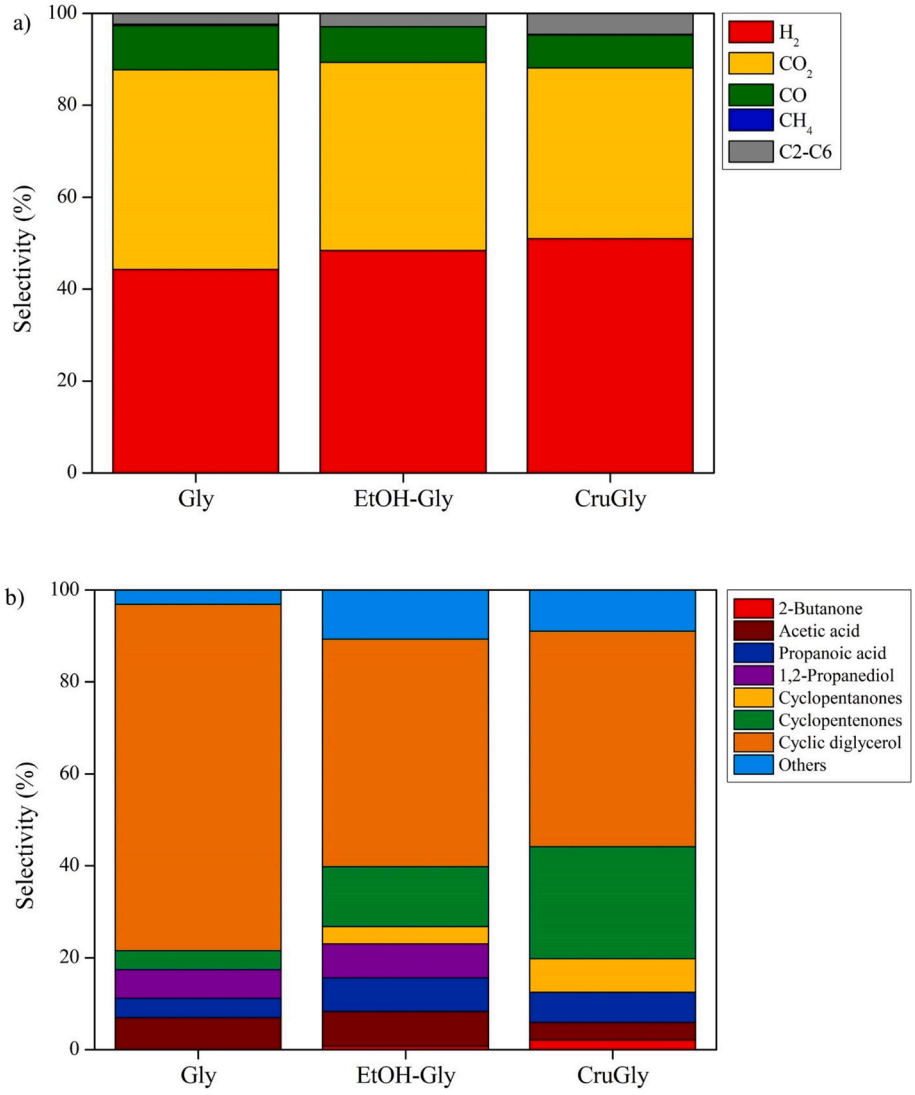

Fig. 9. Selectivity of products in the gas phase (a) and in the liquid phase (b) as the organic feed reagent changes, i.e., Glycerol (Gly), mixture of Ethanol and Glycerol (EtOH-Gly) and Crude Glycerol (CruGly).

cases, resulting in greater selectivity for the target product H_2 and less selectivity for CO_2. The hydrogen selectivity was about 45 % for the case of Gly reaction, higher than the selectivity achieved during Gly SR under the same operating conditions. Saeidabad et al. [82] reported a H_2 selectivity in the range 33.5–38.7 % at 350 °C using 15 % Ni-based catalysts. In fact, according to several studies [83–85], the optimized temperature for Gly SR is 525–725 °C, higher than the 300 °C utilized during the process proposed here. Additionally, the hydrogen produced with respect to the hydrogen fed with glycerol (Performance Index *I*) was 4.8 %, while the thermodynamic value for Gly SR in the same operating conditions was 8.9 % [86]. The index indicated a good performance of the proposed process, especially considering that hydrogen contained in the feedstock was distributed in the multiphase products.

In terms of selectivity towards liquid products, as highlighted in Fig. 9b, the distribution of products varies with the feed composition. Specifically, when pure glycerol is fed, selectivity is directed towards the cyclization products of glycerol itself, namely cyclic diglycerol (or dioxanes), reaching a value of 75 %. Indeed, with a mixture of reactants, either in the presence of ethanol (EtOH-Gly) or water (CruGly), the selectivity towards cyclopentanone and cyclopentenone compounds increased up to about 16 % and 30 %, respectively. The ethanol-glycerol mixture feed scenario is particularly interesting, since a higher selectivity (25 %) was observed towards products of significant importance in the chemical industry, such as propylene glycol, acetic acid, and propanoic acid.

The gaseous mixture consisting of H_2 and biogenic CO_2, with traces of CO and CH_4, can be used in the manufacture of synthetic and renewable fuels in the biorefinery process, or can lead to in-situ bioH_2 as target product after biogenic CO_2 capture. The utilization of gaseous streams comprising hydrogen and carbon dioxide, notably those derived from glycerol, has attracted considerable attention in recent years [87–89]. One interesting application is that the gaseous phase is easily prone to methanation by enriching with green hydrogen or by capturing and recycling the CO_2 until a stoichiometric H_2/CO_2 ratio of 4 is achieved. Synthetic natural gas (SNG) can be used as a clean fuel source or as a precursor to other chemical processes, aligning with the sustainability goals of storing renewable energy within existing gas distribution frameworks [90,91]. Other interesting applications of the H_2-CO_2 stream are the production of renewable methanol via the CO_2 hydrogenation reaction [92,93], or CO synthesis via reverse water–gas shift (rWGS) or high-temperature co-electrolysis, which can then be fed to conventional Fischer-Tropsch process to produce renewable fuels [94,95].

Among the glycerol-based products, increasing attention has been paid to 1,2-propanediol production because of its large range of industrial applications. For example, approximately 45 % of produced 1,2-propane diol is used as a chemical feedstock for unsaturated polyester resin [96]. Moreover, this compound is also used in the food, pharmaceutical, and textile industries because of its versatile and non-toxic nature [97].

Of particular interest is the self-esterification of glycerol, leading to polyglycerol with many different possible applications in the cosmetics, food, polymers and plastic industries. In the plastics sector, hyperbranched polyglycerol can act as surfactants. Linear polyglycerols are commonly used in food industry and diglycerol is used in cosmetics formulations [98].

Additionally, propanoic acid and acetic acid have significant industrial relevance. Because of its antifungal qualities, propanoic acid is utilised as a preservative in the food and feed sectors. Further applications include its significant role as an intermediary in the production of various compounds, such as herbicides and pharmaceuticals [99]. Acetic acid, on the other hand, is a key component in the manufacture of synthetic fibres, plastics, and as a solvent in chemical reactions [100].

Glycerol-based resins bypass the energy-consuming and environmentally harmful processes associated with the conventional production of petroleum-based ones. Renowned for its thermal and mechanical resistance properties, saturated glycerol polyesters resins have applications across various industrial sectors, including composite materials, paints, adhesives, and coatings. In addition, petrol-based resins are banned from food and pharmaceutical additives, while bio-based ones are widely adopted in plasters, drug film coatings and foods [101]. Furthermore, as seen when starting from crude glycerol, the production of a polymeric product with higher thermal stability makes it suitable for applications requiring robust performance under extreme conditions, such as automotive components, electronics, and high-performance composites [102,103].

In summary, the multiphase system outlined in the proposed reaction pathways demonstrates a versatile and efficient method to convert glycerol into a range of valuable chemical products. These products have diverse applications across multiple industries, highlighting the potential of glycerol and sodium metaborate as key raw materials in chemical manufacturing processes. Sodium metaborate provides the water that reacts with glycerol during the initial step producing hydrogen and activates the polymerization reaction, as detailed in the reaction pathway. While current efforts in conventional hydrogen production focus on CO_2 capture, this process produces hydrogen and simultaneously valorizes the carbon present in bio-based feedstocks through the production of value-added products in the biorefinery supply chain. This dual innovation, coupling hydrogen production with carbon valorization represents a significant advancement in hydrogen production technologies.

5. Conclusions

The bio-based building block glycerol, whether in its pure or crude form or when mixed with ethanol, was successfully converted into hydrogen and high-value products through an innovative process. The process involved the use of water and sodium metaborate, a waste product of hydride hydrogen storage technology, at 300 °C, a lower temperature than those currently used in hydrogen production processes. The study highlights the potential of integrating the process in the biorefinery supply chain with biohydrogen production in-situ or upgrading to biofuel. Additionally, key intermediates in the food, pharmaceutical and textile sectors were produced in the liquid phase and a solid polymeric product, which is suitable for high-performance application.

The gas streams contain about 44, 49, and 51 % hydrogen by volume, depending on the feedstock. Hydrogen formed in the reaction also favored the in-situ generation of valuable compounds such as 1,2-propanediol, propanoic acid and cyclopentenones in the liquid phase through the proposed reaction scheme. The solid polymer product, an aliphatic hydrocarbon resin with oxygenated carbon along the saturated chain and aromatic cluster, showed high thermal stability, with decomposition temperatures of 500 °C.

While the study focused on the feasibility of this process, future work should consider optimizing reaction conditions such as temperature, pressure, and feedstock ratios. This work opens up new prospects for the chemical reaction pathways of glycerol and hydrogen production, suggesting a promising avenue for sustainable energy and chemical manufacturing.

CRediT authorship contribution statement

Alessandra Di Nardo: Writing – original draft, Methodology, Investigation, Data curation. **Gianluca Landi:** Writing – review & editing, Formal analysis. **Giuseppina Luciani:** Writing – review & editing, Methodology. **Maria Portarapillo:** Writing – review & editing, Methodology. **Giovanna Ruoppolo:** Resources, Formal analysis. **Danilo Russo:** Writing – review & editing. **Armando Zarrelli:** Writing – original draft, Investigation, Formal analysis. **Almerinda Di Benedetto:** Writing – review & editing, Visualization, Validation, Supervision, Conceptualization.

Declaration of competing interest

The authors declare that they have no known competing financial interests or personal relationships that could have appeared to influence the work reported in this paper.

Acknowledgements

The authors acknowledge Mr. Andrea Capuozzo, Mr. Fernando Stanzione, and Mr. Luigi Stanzione, for their kind assistance with GC-MS analysis and Mr. Luigi Cortese for his technical support with SEM measurements.

Funding

This research did not receive any specific grant from funding agencies in the public, commercial, or not-for-profit sectors.

Appendix A. Supplementary data

Supplementary data to this article can be found online at https://doi.org/10.1016/j.cej.2024.156634.

Data availability

Data will be made available on request.

References

[1] J. De Vrieze, K. Verbeeck, I. Pikaar, J. Boere, A. Van Wijk, K. Rabaey, W. Verstraete, The hydrogen gas bio-based economy and the production of renewable building block chemicals, food and energy, N, Biotechnol. 55 (2020) 12–18, https://doi.org/10.1016/j.nbt.2019.09.004.

[2] S.C. Khor, M. Jusoh, Z.Y. Zakaria, Hydrogen production from steam and dry reforming of methane-ethane-glycerol: A thermodynamic comparative analysis, Chem. Eng. Res. Des. 180 (2022) 178–189, https://doi.org/10.1016/j.cherd.2022.02.015.

[3] Y. Liu, B. Zhong, A. Lawal, Recovery and utilization of crude glycerol, a biodiesel byproduct, RSC Adv 12 (2022) 27997–28008, https://doi.org/10.1039/d2ra05090k.

[4] D. Russo, M. Portarapillo, A. Di Benedetto, Flash point of biodiesel/glycerol/alcohol mixtures for safe processing and storage, J. Loss Prev. Process Ind. 83 (2023) 105077, https://doi.org/10.1016/j.jlp.2023.105077.

[5] S. Pradhan, R.S. Malani, Assessment of farm-level biodiesel unit—a potential alternative for sustainable future, Handbook of Biofuels (2022) 377–396, https://doi.org/10.1016/B978-0-12-822810-4.00019-1.

[6] T. Attarbachi, M.D. Kingsley, V. Spallina, New trends on crude glycerol purification: A review, Fuel 340 (2023) 127485, https://doi.org/10.1016/j.fuel.2023.127485.

[7] S.C. D'Angelo, A. Dall'Ara, C. Mondelli, J. Pérez-Ramírez, S. Papadokonstantakis, Techno-Economic Analysis of a Glycerol Biorefinery, ACS Sustain. Chem. Eng. 6 (2018) 16563–16572. doi: 10.1021/acssuschemeng.8b03770.

[8] Z. Pirzadi, F. Meshkani, From glycerol production to its value-added uses: A critical review, Fuel 329 (2022) 125044, https://doi.org/10.1016/j.fuel.2022.125044.

[9] P. Koranian, Q. Huang, A.K. Dalai, R. Sammynaiken, Chemicals Production from Glycerol through Heterogeneous Catalysis: A Review, Catalysts 12 (2022) 897, https://doi.org/10.3390/catal12080897.

[10] F. Qureshi, M. Yusuf, A.A. Pasha, H.W. Khan, B. Imteyaz, K. Irshad, Sustainable and energy efficient hydrogen production via glycerol reforming techniques: A review, Int. J. Hydrog. Energy 47 (2022) 41397–41420, https://doi.org/10.1016/j.ijhydene.2022.04.010.

[11] G. Ruoppolo, G. Landi, A. Di Benedetto, Glycerol dehydration to acrolein over supported vanadyl orthophosphates catalysts, Catalysts 10 (2020) 673, https://doi.org/10.3390/catal10060673.

[12] A. Abdullah, A. Zuhairi Abdullah, M. Ahmed, J. Khan, M. Shahadat, K. Umar, M. A. Alim, A review on recent developments and progress in sustainable acrolein production through catalytic dehydration of bio-renewable glycerol, J. Clean Prod. 341 (2022) 130876, https://doi.org/10.1016/j.jclepro.2022.130876.

[13] F. Fernandes Barbosa, T. Pinheiro Braga, Catalytic Conversion of Glycerol to Acetol and Acrolein Using Metal Oxides: Surface Reactions, Prospects and Challenges, ChemCatChem 15 (2023), https://doi.org/10.1002/cctc.202200950.

[14] D.K. Pandey, P. Biswas, Review of the Development of Heterogeneous Catalysts for Liquid and Vapor Phase Hydrogenolysis of Glycerol to Propylene Glycol (1,2-Propanediol): State-of-the-Art and Outlook, Ener. Fuel. 37 (2023) 6879–6906, https://doi.org/10.1021/acs.energyfuels.2c03806.

[15] G. Luciani, G. Ruoppolo, G. Landi, V. Gargiulo, M. Alfè, A. Di Benedetto, Glycerol Hydrogenolysis to 1,2-Propanediol over Novel Cu/ZrO2 Catalysts, Catalysts 12 (2022) 72, https://doi.org/10.3390/catal12010072.

[16] J. Chen, M. Wang, S. Zhang, Y. Wang, J. Hua, X. Meng, Q. Xia, J. Qiu, S. Liu, High performance Pt/Nb2W3O14 catalyst for glycerol valorization to 1,3-propanediol, Chem. Eng. J. 486 (2024) 150327, https://doi.org/10.1016/j.cej.2024.150327.

[17] R. Nguyen, N. Galy, A.K. Singh, F. Paulus, D. Stöbener, C. Schlesener, S. K. Sharma, R. Haag, C. Len, A simple and efficient process for large scale glycerol oligomerization by microwave irradiation, Catalysts 7 (2017) 123, https://doi.org/10.3390/catal7040123.

[18] D. Kansy, K. Bosowska, K. Czaja, A. Poliwoda, The formation of glycerol oligomers with two new types of end groups in the presence of a homogeneous alkaline catalyst, Polymers (basel) 11 (2019) 144, https://doi.org/10.3390/polym11010144.

[19] G.P.S. Ibrahim, A.M. Isloor, A.M. Inamuddin, A.F. Asiri, R. Ismail, M.I.A. Kumar, Performance intensification of the polysulfone ultrafiltration membrane by blending with copolymer encompassing novel derivative of poly(styrene-co-maleic anhydride) for heavy metal removal from wastewater, Chem. Eng. J. 353 (2018) 425–435, https://doi.org/10.1016/j.cej.2018.07.098.

[20] H. Wang, H. Li, C.K. Lee, N.S. Mat Nanyan, G.S. Tay, A systematic review on utilization of biodiesel-derived crude glycerol in sustainable polymers preparation, Int. J. Biol. Macromol. (2024) 129536, https://doi.org/10.1016/j.ijbiomac.2024.129536.

[21] A. Hejna, P. Kosmela, K. Formela, Ł. Piszczyk, J.T. Haponiuk, Potential applications of crude glycerol in polymer technology–Current state and perspectives, Renew. Sustain. Energy Rev. 66 (2016) 449–475, https://doi.org/10.1016/j.rser.2016.08.020.

[22] S. Goyal, N.B. Hernández, E.W. Cochran, An update on the future prospects of glycerol polymers, Polym. Int. 70 (2021) 911–917, https://doi.org/10.1002/pi.6209.

[23] M.A. Ahmad, A.M. Quraishi, S. Jagnandan, A. Jagnandan, J.H. Baker, M. I. Ahamed, M.M. Abdullah, H.B. Albargi, R. Nizam, S. Pandey, Understanding into atomic structures and electronic properties from the analysis of intramolecular junctions in carbon nanotubes, Mater. Today Commun. 38 (2024) 108096, https://doi.org/10.1016/j.mtcomm.2024.108096.

[24] A. Di Benedetto, M. Portarapillo, G. Landi, G. Luciani, Process for green hydrogen production. WO2023105545A1, 2023.

[25] A. Di Nardo, M. Portarapillo, D. Russo, G. Luciani, G. Landi, G. Ruoppolo, A. Pezzella, A. Di Benedetto, Cyan Hydrogen Process: A New Route for Simultaneous Hydrogen Production and Carbon Valorization, ACS Omega 9 (2024) 7793–7805, https://doi.org/10.1021/acsomega.3c07277.

[26] N. Klopčič, I. Grimmer, F. Winkler, M. Sartory, A. Trattner, A review on metal hydride materials for hydrogen storage, J. Energy Storage 72 (2023) 108456, https://doi.org/10.1016/j.est.2023.108456.

[27] Grand View Reserach, Glycerol Market Size, Share & Trends, accessed September 11, 2024, Analysis 2021–2027 (2023), https://www.grandviewresearch.com/industry-analysis/glycerol-market.

[28] OECD/FAO, OECD-FAO Agricultural Outlook 2021-2030, OECD, Paris, 2021. doi: 10.1787/19428846-en.

[29] K. Mathiazhakan, D. Ayed, R.D. Tyagi, Kinetics of lipid production at lab scale fermenters by a new isolate of Yarrowia lipolytica SKY7, Bioresour. Technol. 221 (2016) 234–240, https://doi.org/10.1016/j.biortech.2016.09.015.

[30] Y. Xiao, A. Varma, Conversion of Glycerol to Hydrocarbon Fuels via Bifunctional Catalysts, ACS Energy Lett. 1 (2016) 963–968, https://doi.org/10.1021/acsenergylett.6b00421.

[31] A.K. Figen, S. Pikin, Parametric investigation on anhydrous sodium metaborate (NaBO2) synthesis from concentrated tincal, Adv. Powder Technol. 21 (2010) 513–520, https://doi.org/10.1016/j.apt.2010.01.012.

[32] J. Coates, Interpretation of Infrared Spectra, A Practical Approach, R.A. Meyers (Ed.), Chichester, 2006.

[33] I. Zojaji, A. Esfandiarian, J. Taheri-Shakib, Toward molecular characterization of asphaltene from different origins under different conditions by means of FT-IR spectroscopy, Adv. Colloid Interface Sci. 289 (2021) 102314, https://doi.org/10.1016/j.cis.2020.102314.

[34] T. Liang, Z.W. Zhan, Y.R. Zou, Molecular Simulation of Resin and the Calculation of Molecular Bond Energy, ACS Omega 6 (2021) 28254–28262, https://doi.org/10.1021/acsomega.1c04342.

[35] T. Liang, X.H. Lin, Y.R. Zou, Z.W. Zhan, P. Peng, Elucidating the chemical structures of petroleum resin using solid-state 13C NMR, Chem. Geol. 630 (2023) 121492, https://doi.org/10.1016/j.chemgeo.2023.121492.

[36] J. Jiang, S. Zhang, P. Longhurst, W. Yang, S. Zheng, Molecular structure characterization of bituminous coal in Northern China via XRD, Raman and FTIR spectroscopy, Spectrochim. Acta A Mol. Biomol. Spectrosc. 255 (2021) 119724, https://doi.org/10.1016/j.saa.2021.119724.

[37] S. Ok, N. Rajasekaran, M.A. Sabti, G.A. Joseph, Spectroscopic Analysis of Crude Oil Asphaltenes at Molecular Level, Petr. Chem. 60 (2020) 802–809, https://doi.org/10.1134/S0965544120070117.

[38] A.D. Mohammed, D.A. Young, H.C.M. Vosloo, Synthesis of high-performance superabsorbent glycerol acrylate-cross-linked poly (acrylic acid), Res. Chem. Intermediat. 43 (2017) 2187–2200, https://doi.org/10.1007/s11164-016-2754-x.

[39] X. Xiao, Z. Chen, B. Chen, H/C atomic ratio as a smart linkage between pyrolytic temperatures, aromatic clusters and sorption properties of biochars derived from diverse precursory materials, Sci. Rep. 6 (2016), https://doi.org/10.1038/srep22644.

[40] S. Wijitkosum, T. Sriburi, Aromaticity, polarity, and longevity of biochar derived from disposable bamboo chopsticks waste for environmental application, Heliyon 9 (2023) e19831.

[41] S.I. Andersen, J.G. Speight, Petroleum resins: Separation, character, and role in petroleum, Pet. Sci. Technol. 19 (2001) 1–34, https://doi.org/10.1081/LFT-100001223.

[42] P.M. Spiecker, K.L. Gawrys, C.B. Trail, P.K. Kilpatrick, Effects of petroleum resins on asphaltene aggregation and water-in-oil emulsion formation, Coll. Surf. A Physicochem. Eng. Asp. 220 (2003) 9–27, https://doi.org/10.1016/S0927-7757(03)00079-7.

[43] J.K. Kim, Y. Ryu, K.-H. Lee, The aromatic hydrocarbon resins with various hydrogenation degrees Part 1. The phase behavior and miscibility with polybutadiene and with polystyrene, Polymer (guildf) 41 (2000) 5195–5205, https://doi.org/10.1016/S0032-3861(99)00614-X.

[44] D. Zhou, X. Chen, J. Liang, X. Wei, C. Wu, W. Li, L. Wang, High-Temperature Stability and Pyrolysis Kinetics and Mechanism of Bio-Based and Petro-Based Resins Using TG-FTIR/MS, Ind. Eng. Chem. Res. 60 (2021) 13774–13789, https://doi.org/10.1021/acs.iecr.1c02535.

[45] V. Venezia, G. Pota, B. Silvestri, G. Vitiello, P. Di Donato, G. Landi, V. Mollo, M. Verrillo, S. Cangemi, A. Piccolo, G. Luciani, A study on structural evolution of hybrid humic Acids-SiO2 nanostructures in pure water: Effects on physico-chemical and functional properties, Chemosphere 287 (2022) 131985, https://doi.org/10.1016/j.chemosphere.2021.131985.

[46] K. Kaur, R. Kaur, H. Kaur, A systematic review of lignocellulosic biomass for remediation of environmental pollutants, Appl. Surf. Sci. Adv. 19 (2024) 100547, https://doi.org/10.1016/j.apsadv.2023.100547.

[47] A. Fasolini, D. Cespi, T. Tabanelli, R. Cucciniello, F. Cavani, Hydrogen from renewables: A case study of glycerol reforming, Catalysts 9 (2019) 722, https://doi.org/10.3390/catal9090722.

[48] S. Basu, A.K. Sen, A Review on Catalytic Dehydration of Glycerol to Acetol, ChemBioEng Rev. 8 (2021) 633–653, https://doi.org/10.1002/cben.202100009.

[49] A. Torres, H. Shi, B. Subramaniam, R.V. Chaudhari, Aqueous-Phase Glycerol Catalysis and Kinetics with in Situ Hydrogen Formation, ACS Sustain. Chem. Eng. 7 (2019) 11323–11333, https://doi.org/10.1021/acssuschemeng.9b00807.

[50] C. Su, S. Zhou, S. Wu, M. Gao, W. Zhang, Z. Ma, L. Yan, F. Zhang, J. Chen, H. Li, J. Liu, H. Zheng, Highly efficient dehydration of polyols: In-situ Brønsted acid from boron phosphate catalyst, Chem. Eng. J. 483 (2024) 149273, https://doi.org/10.1016/j.cej.2024.149273.

[51] H. Atiyeh, B. Davis, Separation of sodium metaborate from sodium borohydride using nanofiltration membranes for hydrogen storage application, Int. J. Hydrog. Energy 32 (2007) 229–236, https://doi.org/10.1016/j.ijhydene.2006.06.003.

[52] A.Z. Halimehjani, H. Gholami, M.R. Saidi, Boric acid/glycerol as an efficient catalyst for regioselective epoxide ring opening by aromatic amines in water, Green Chem. Lett. Rev. 5 (2012) 1–5, https://doi.org/10.1080/17518253.2011.572297.

[53] J. Chaminand, L. aurent Djakovitch, P. Gallezot, P. Marion, C. Pinel, C. Rosier, Glycerol hydrogenolysis on heterogeneous catalysts, Green Chem. 6 (2004) 359. doi: 10.1039/b407378a.

[54] M.E. Sad, H.A. Duarte, Ch. Vignatti, C.L. Padró, C.R. Apesteguía, Steam reforming of glycerol: Hydrogen production optimization, Int. J. Hydrog. Energy 40 (2015) 6097–6106, https://doi.org/10.1016/j.ijhydene.2015.03.043.

[55] T. Valliyappan, D. Ferdous, N.N. Bakhshi, A.K. Dalai, Production of Hydrogen and Syngas via Steam Gasification of Glycerol in a Fixed-Bed Reactor, Top Catal. 49 (2008) 59–67, https://doi.org/10.1007/s11244-008-9062-7.

[56] C.A. Schwengber, H.J. Alves, R.A. Schaffner, F.A. da Silva, R. Sequinel, V.R. Bach, R.J. Ferracin, Overview of glycerol reforming for hydrogen production, Renew. Sustain. Energy Rev. 58 (2016) 259–266, https://doi.org/10.1016/j.rser.2015.12.279.

[57] R.D. Cortright, R.R. Davda, J.A. Dumesic, Hydrogen from catalytic reforming of biomass-derived hydrocarbons in liquid water, Nature 418 (2002) 964–967, https://doi.org/10.1038/nature01009.

[58] F. Pompeo, G. Santori, N.N. Nichio, Hydrogen and/or syngas from steam reforming of glycerol. Study of platinum catalysts, Int. J. Hydrog. Energy 35 (2010) 8912–8920, https://doi.org/10.1016/j.ijhydene.2010.06.011.

[59] M. Główka, T. Krawczyk, New Trends and Perspectives in Production of 1,2-Propanediol, ACS Sustain. Chem. Eng. 11 (2023) 7274–7287, https://doi.org/10.1021/acssuschemeng.3c01018.

[60] M. Akiyama, S. Sato, R. Takahashi, K. Inui, M. Yokota, Dehydration–hydrogenation of glycerol into 1,2-propanediol at ambient hydrogen pressure, Appl Catal A Gen 371 (2009) 60–66, https://doi.org/10.1016/j.apcata.2009.09.029.

[61] J. Svachula', J. Tichp, J. Machek, Kinetics of Hydrogenation of Acrylic Acid to Propionic Acid on a Copper Catalyst, Appl. Catal. 38 (1988) 53–59. doi: doi: 10.1016/S0166-9834(00)80985-9.

[62] K. Zhou, C. Sun, X. Liu, Directed glycerol conversion to 2,5-hexanedione and more advanced poly-oxygenates as platform chemicals and high energy–density fuel additives, Chem. Eng. J. 430 (2022) 132981, https://doi.org/10.1016/j.cej.2021.132981.

[63] K. Koichumanova, A.K.K. Vikla, R. Cortese, F. Ferrante, K. Seshan, D. Duca, L. Lefferts, In situ ATR-IR studies in aqueous phase reforming of hydroxyacetone on Pt/ZrO2 and Pt/AlO(OH) catalysts: The role of aldol condensation, Appl. Catal. B 232 (2018) 454–463, https://doi.org/10.1016/j.apcatb.2018.03.090.

[64] J. Woodroffe, B.G. Harvey, Synthesis of Bio-Based Methylcyclopentadiene from 2,5-Hexanedione: A Sustainable Route to High Energy Density Jet Fuels, ChemSusChem 14 (2021) 339–343, https://doi.org/10.1002/cssc.202002209.

[65] R. Wang, Y. Liu, G. Li, A. Wang, X. Wang, Y. Cong, T. Zhang, N. Li, Direct Synthesis of Methylcyclopentadiene with 2,5-Hexanedione over Zinc Molybdates, ACS Catal. 11 (2021) 4810–4820, https://doi.org/10.1021/acscatal.1c00223.

[66] T. Adachi, E. Kurniawan, T. Hara, R. Takahashi, Y. Yamada, S. Sato, Vapor-phase intramolecular aldol condensation of 2,5-hexanedione over yttrium zirconate catalyst, Appl. Catal. A Gen. 685 (2024) 119887, https://doi.org/10.1016/j.apcata.2024.119887.

[67] S. Nishimura, S. Ohmatsu, K. Ebitani, Selective synthesis of 3-methyl-2-cyclopentenone via intramolecular aldol condensation of 2,5-hexanedione with γ-Al2O3/AlOOH nanocomposite catalyst, Fuel Process. Technol. 196 (2019) 106185, https://doi.org/10.1016/j.fuproc.2019.106185.

[68] T. Vilarinho-Franco, A. Teyssier, R. Tenu, J. Pécaut, J. Delmas, M. Heitzmann, P. Capron, J.J. Counioux, C. Goutaudier, Solid-liquid equilibria in the ternary system NaBO2-NaOH-H2O thermal behavior of double salts, Fluid Phase Equilib. 360 (2013) 212–221, https://doi.org/10.1016/j.fluid.2013.09.035.

[69] Y. Liu, G. Li, Y. Hu, A. Wang, F. Lu, J.-J. Zou, Y. Cong, N. Li, T. Zhang, Integrated Conversion of Cellulose to High-Density Aviation Fuel, Joule 3 (2019) 1028–1036, https://doi.org/10.1016/j.joule.2019.02.005.

[70] A. Zamboulis, E.A. Nakiou, E. Christodoulou, D.N. Bikiaris, E. Kontonasaki, L. Liverani, A.R. Boccaccini, Polyglycerol Hyperbranched Polyesters: Synthesis, Properties and Pharmaceutical and Biomedical Applications, Int. J. Mol. Sci. 20 (2019) 6210, https://doi.org/10.3390/ijms20246210.

[71] O. Valerio, M. Misra, A.K. Mohanty, Poly(glycerol- co-diacids) Polyesters: From Glycerol Biorefinery to Sustainable Engineering Applications, A Review, ACS Sustain. Chem. Eng. 6 (2018) 5681–5693, https://doi.org/10.1021/acssuschemeng.7b04837.

[72] A. Bhargava, S. Shelke, M. Dilkash, N.S. Chaubal-Durve, P.D. Patil, S.S. Nadar, D. Marghade, M.S. Tiwari, A comprehensive review on catalytic etherification of glycerol to value-added products, Rev. Chem. Eng. 39 (2022) 1187–1226, https://doi.org/10.1515/revce-2021-0074.

[73] P. Palanychamy, S. Lim, Y.H. Yap, L.K. Leong, Critical Review of the Various Reaction Mechanisms for Glycerol Etherification, Catalysts 12 (2022) 1487, https://doi.org/10.3390/catal12111487.

[74] S. Tanpichai, F. Phoothong, A. Boonmahitthisud, Superabsorbent cellulose-based hydrogels cross-liked with borax, Sci. Rep. 12 (2022) 8920, https://doi.org/10.1038/s41598-022-12688-2.

[75] V.-L. Yfanti, A.A. Lemonidou, Mechanistic study of liquid phase glycerol hydrodeoxygenation with in-situ generated hydrogen, J. Catal. 368 (2018) 98–111, https://doi.org/10.1016/j.jcat.2018.09.036.

[76] A.-Y. Yin, X.-Y. Guo, W.-L. Dai, K.-N. Fan, The synthesis of propylene glycol and ethylene glycol from glycerol using Raney Ni as a versatile catalyst, Green Chem. 11 (2009) 1514, https://doi.org/10.1039/b913395j.

[77] Y. Liu, J. Liu, Z. Xing, X. Zhang, C. Luo, W. Yan, X. Jin, Kinetic Modeling of Glycerol Hydrogenolysis: A Short Review, Catalysts 13 (2022) 23, https://doi.org/10.3390/catal13010023.

[78] Z. Li, B.D. Kay, Z. Dohnálek, Dehydration and dehydrogenation of ethylene glycol on rutile TiO2(110), Phys. Chem. Chem. Phys. 15 (2013) 12180, https://doi.org/10.1039/c3cp50687h.

[79] X. Zhu, Z. Guo, W. Cen, B. Mao, Ethylene Polymerization Using Improved Polyethylene Catalyst, Chin. J. Chem. Eng. 19 (2011) 52–56, https://doi.org/10.1016/S1004-9541(09)60176-2.

[80] A. Goller, J. Obenauf, W.P. Kretschmer, R. Kempe, The Highly Controlled and Efficient Polymerization of Ethylene, Angew. Chem. Int. Ed. 62 (2023), https://doi.org/10.1002/anie.202216464.

[81] S. Kobayashi, H. Higashimura, Oxidative polymerization of phenols revisited, Prog. Polym. Sci. 28 (2003) 1015–1048, https://doi.org/10.1016/S0079-6700(03)00014-5.

[82] N.G. Saeidabad, Y.S. Noh, A.A. Eslami, H.T. Song, H.D. Kim, A. Fazeli, D.J. Moon, A review on catalysts development for steam reforming of biodiesel derived glycerol; promoters and supports, Catalysts 10 (2020) 1–22, https://doi.org/10.3390/catal10080910.

[83] A. Zarei Senseni, M. Rezaei, F. Meshkani, Glycerol steam reforming over noble metal nanocatalysts, Chem. Eng. Res. Des. 123 (2017) 360–366, https://doi.org/10.1016/j.cherd.2017.05.020.

[84] A.G. Adeniyi, J.O. Ighalo, A review of steam reforming of glycerol, Chem. Pap. 73 (2019) 2619–2635, https://doi.org/10.1007/s11696-019-00840-8.

[85] M.S. Macedo, M.A. Soria, L.M. Madeira, Process intensification for hydrogen production through glycerol steam reforming, Renew. Sustain. Energy Rev. 146 (2021), https://doi.org/10.1016/j.rser.2021.111151.

[86] A. Di Nardo, M. Portarapillo, D. Russo, A. Di Benedetto, Hydrogen production via steam reforming of different fuels: thermodynamic comparison, Int. J. Hydrog. Energy (2023), https://doi.org/10.1016/j.ijhydene.2023.11.215.

[87] H. Zhao, C. Xu, T. Wang, Production of methane from biomass glycerol through coupling of steam reforming and methanation on Ni-Mn/Al2O3, Sustain. Chem. Pharm. 13 (2019) 100150, https://doi.org/10.1016/j.scp.2019.100150.

[88] C. Venu, D. Palanisamy, S. Jaganathan, S. Rajendran, Production and evaluation of syngas derived from glycerol using aqueous phase reforming for fueling compression ignition engines, Renew. Energy 219 (2023) 119594, https://doi.org/10.1016/j.renene.2023.119594.

[89] A. Serrera, F.J. Gutiérrez Ortiz, P. Ollero, Syngas methanation from the supercritical water reforming of glycerol, Energy 76 (2014) 584–592, https://doi.org/10.1016/j.energy.2014.08.056.

[90] J. Ren, H. Lou, N. Xu, F. Zeng, G. Pei, Z. Wang, Methanation of CO/CO2 for power to methane process: Fundamentals, status, and perspectives, J. Energy Chem. 80 (2023) 182–206, https://doi.org/10.1016/j.jechem.2023.01.034.

[91] J. Ashok, S. Pati, P. Hongmanorom, Z. Tianxi, C. Junmei, S. Kawi, A review of recent catalyst advances in CO2 methanation processes, Catal. Today 356 (2020) 471–489, https://doi.org/10.1016/j.cattod.2020.07.023.
[92] Q.I. Roode-Gutzmer, D. Kaiser, M. Bertau, Renewable Methanol Synthesis, ChemBioEng Rev. 6 (2019) 209–236, https://doi.org/10.1002/cben.201900012.
[93] S. Sollai, A. Porcu, V. Tola, F. Ferrara, A. Pettinau, Renewable methanol production from green hydrogen and captured CO2: A techno-economic assessment, J. CO2 Util. 68 (2023) 102345, https://doi.org/10.1016/j.jcou.2022.102345.
[94] G. Zang, P. Sun, A.A. Elgowainy, A. Bafana, M. Wang, Performance and cost analysis of liquid fuel production from H2 and CO2 based on the Fischer-Tropsch process, J. CO2 Util. 46 (2021) 101459, https://doi.org/10.1016/j.jcou.2021.101459.
[95] S. Pratschner, M. Hammerschmid, S. Müller, F. Winter, Evaluation of CO2 sources for Power-to-Liquid plants producing Fischer-Tropsch products, J. CO2 Util. 72 (2023) 102508, https://doi.org/10.1016/j.jcou.2023.102508.
[96] J.B. Restrepo, C.D. Paternina-Arboleda, A.J. Bula, 1,2—Propanediol Production from Glycerol Derived from Biodiesel's Production: Technical and Economic Study, Energies (basel) 14 (2021) 5081, https://doi.org/10.3390/en14165081.
[97] B.S. Shrirame, A.R. Varma, S.S. Sahoo, K. Gayen, S.K. Maity, Techno-commercial viability of glycerol valorization to 1,2- and 1,3-propanediol using pinch technology, Biomass Bioenerg. 177 (2023) 106943, https://doi.org/10.1016/j.biombioe.2023.106943.
[98] N. Ebadipour, S. Paul, B. Katryniok, F. Dumeignil, Alkaline-Based Catalysts for Glycerol Polymerization Reaction: A Review, Catalysts 10 (2020) 1021, https://doi.org/10.3390/catal10091021.
[99] A.M. Abdel-Azeem, F.A. Abo Nouh, S.A. Gezaf, A.M.G. Darwish, M.A. Abdel-Azeem, Propionic acid chemistry and production, in: Valorization of Biomass to Bioproducts, Elsevier, 2023: pp. 3–15. doi: 10.1016/B978-0-12-822888-3.00011-6.
[100] Z. Xu, Z. Shi, L. Jiang, Acetic and Propionic Acids, in, Comprehensive Biotechnology, Elsevier (2011) 189–199, https://doi.org/10.1016/B978-0-08-088504-9.00162-8.
[101] V. Fakhri, C.-H. Su, M. Tavakoli Dare, M. Bazmi, A. Jafari, V. Pirouzfar, Harnessing the power of polyol-based polyesters for biomedical innovations: synthesis, properties, and biodegradation, J. Mater. Chem. B 11 (2023) 9597–9629, https://doi.org/10.1039/D3TB01186K.
[102] Y. Qi, Z. Weng, K. Zhang, J. Wang, S. Zhang, C. Liu, X. Jian, Magnolol-based bio-epoxy resin with acceptable glass transition temperature, processability and flame retardancy, Chem. Eng. J. 387 (2020) 124115, https://doi.org/10.1016/j.cej.2020.124115.
[103] X. Liu, W. Xin, J. Zhang, Rosin-based acid anhydrides as alternatives to petrochemical curing agents, Green Chem. 11 (2009) 1018, https://doi.org/10.1039/b903955d.